Celal Bayar University Journal of Science

Chemical Inferences Drawn From Basalt Volcanic Pumice

Ruhan Benlikaya[1]*, Mehmet Kahrıman[2]

[1] Balıkesir University, Dept. of Secondary Science and Mathematics Education, Balikesir, Türkiye
[2] Private Tunafen Anatolian High School, Ankara, Türkiye
* ruhan@balikesir.edu.tr
* Orcid: 0000-0002-1731-8846

Received: 9 September 2021
Accepted: 27 May 2022
DOI: 10.18466/cbayarfbe.993131

Abstract

The idea to conduct this study came out with the purpose of responding to two questions concerning the Kula Geopark. The questions were as follows: how the wettability of the natural pumice sample with spongy structure taken from this site is and how it can be altered. With this end in view, firstly the pumice samples were characterized by X-ray Fluorescence Spectroscopy, Fourier Transform Infrared Spectroscopy and Scanning Electron Microscopy analyses. Next, after observing super hydrophilic nature of the pumice with porous structure containing various metal oxides, the samples were coated with copper stearate dispersion using a spraying method. And then the wettability properties of the copper stearate-treated samples were determined via contact angles. Given the data obtained, the wettability phenomena of these samples were discussed in terms of wettability models.

Keywords: Contact angle, Cassie Baxter, Volcanic pumice, Wenzel, Wettability.

1. Introduction

Pumice is a silicate-based, spongy-looking rock formed after volcanic activities. It can be found in a variety of colors from white to gray, red and brown to black. Turkey has 2.2 billion tons of pumice reserves [1]. There are important pumice deposits in the provinces of Manisa, Kayseri, Van, Bitlis, Ağrı, Osmaniye and Nevşehir [2]. The Kula Volcano of the youngest volcanic activity in Manisa is one of 14 volcanoes in our country. Around 80 volcanic edifices are located on the North flank of the Alaşehir Graben, Manisa [3]. The area of the Kula Volcano extends 15 km and 40 km in the north-south direction and in the west-east direction, respectively. In 2013, the volcanic field was accepted as the first geopark in Turkey by UNESCO and the 58th in Europe as Gürsoy et al. stated [4].

Quaternary volcanism in the Kula region started approximately 2 million years ago. This volcanism occurred due to the stress tectonics that started in the Pliocene in Western Anatolia. It is suggested that the mentioned volcanism is related to the rifting (tensions) that probably caused the formation of the Alaşehir graben in the region [5]. The common eruption products of these volcanoes are mostly alkaline type of pyroclastic materials such as basaltic lava flows, tephra and slag. Basaltic lava flows and pyroclastic cones form the most common forms of volcanic relief in the Kula volcanic field, which is one of the youngest examples of volcanic topography in Anatolia [5].

There have been many studies on various applications of modified/coated/natural volcanic pumice samples in mainly two fields: construction industry (cement replacement material [6] and heat-insulating material [7]) and water/wastewater/soil/air treatment (production of hybrid catalyst [8], removal of various substances such as cadmium [9], natural organic matter [10], selenium [11], disinfection by-product precursors [12], lead and copper ions [13], etc. from at least one of these medium). In some of these studies, the volcanic pumice samples supplied from the Kula region have also been used [10-13]. However, there is no study on the wettability of the pumice samples. The aim of this study is to characterize the volcanic pumice at the Kula region and to discuss wetting phenomena of the pumice samples in terms of wettability models by changing its surface property.

1.1 Theory

Surface wettability is the ability of a solid surface to maintain contact with a liquid as a result of competing of adhesion and cohesion forces. The wettability of solid surface depends strongly on both its chemical

Celal Bayar University Journal of Science
Volume 18, Issue 2, 2022, p 225-231
Doi: 10.18466/cbayarfbe.993131

composition and surface morphology. The slope of the line drawn tangent to the liquid drop from the intersection of solid, liquid and air (vapor) phases between a solid surface and a liquid drop on this solid surface is defined as the "contact angle" [14]. To explain the geometry of the surfaces repelling water and oil, mainly 3 different mathematical approximation models are widely used: Young, Wenzel and Cassie-Baxter, of which schematics are shown in Figure 1.

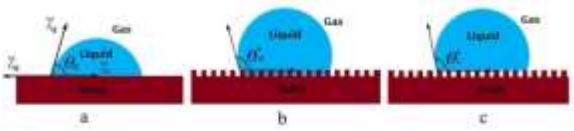

Figure 1. A droplet in the Young state on a smooth solid surface (a), collapsed in the Wenzel state (b), suspended in the Cassie-Baxter state (c).

The first equation and the most basic theory for wettability (1805) is Young's equation which explains the static contact angle (θ_Y) of the liquid on the solid surface having a homogeneous, smooth, and infinite flat ideal rigidity. Surface tension among the interfaces of solid-liquid, liquid-gas and solid-gas is balanced according to the equation (1.1) on horizontal direction, the model of which is given in Figure 1a.

$$cos\theta_Y = (\gamma_{sg} - \gamma_{sl})/\gamma_{lg} \quad \textbf{(1.1)}$$

In this equation, γ_{sg}, γ_{sl} and γ_{lg} represent interface tensions of solid–gas, solid–liquid, and liquid–gas, respectively [14]. The contact angle of a liquid drop on the solid surface depends on equilibrium between cohesive forces (γ_{lg}) in the liquid and adhesive forces (γ_{sg} and γ_{sl}) between the pairs (s-l and s-g) in Young's equation.

Wenzel (1936) revealed that surface roughness (r) can significantly alter the contact angle of water; its model can be seen in Figure 1b. Drops become sticky to the surface when the liquid fully wets it as a result of penetrating to the grooves of rough surface on solid [15]. The existence of a rough structure at a solid surface causes an increase in the real superficial area of this surface. This makes that the actual solid–liquid contact area is larger than the apparent geometric contact area. Thus, hydrophobicity/hydrophilicity of the surface increases depending on geometry. The equation of the contact angle (θ_W) in Wenzel view is given in the equation (1.2) as

$$cos\theta_W = r.\frac{\gamma_{sg}-\gamma_{sl}}{\gamma_{lg}} = r.cos\theta_Y \quad \textbf{(1.2)}$$

where r is the roughness factor, representing the ratio of the actual area on rough surface to apparent geometry area. The r factor will enhance the hydrophobicity/the hydrophilicity when the value of θ_y is more/less than 90° [15, 16].

The roughness effect on the behavior of the drop on the surface was explained by Cassie-Baxter (1944). Unlike Wenzel, wetting is assumed to be heterogeneous in this model, Figure 1c. The contact area between liquid and solid is minimized due to air trapped in the surface voids by the liquid, while the one between liquid and air is maximized. Thus, liquid is forced to form spherical drops [16]. Depending upon Young's equation, the relationship between Cassie-Baxter contact angle (θ_{CB}) and θ_Y can be given with the equation (1.3) below

$$cos\theta_{CB} = f.(cos\theta_Y + 1) - 1 \quad \textbf{(1.3)}$$

where f is the ratio of solid–liquid interface contact area and actual surface area under droplet within the unit area [14, 16]. In Cassie impregnating model, droplet penetrates completely or partially through the gaps between microstructures while not penetrate or only partially penetrates to the nanostructures [17, cited in 15]. This model can be thought of as an intermediate state between Wenzel and Cassie-Baxter models [17]. The wetted area in the model is greater than the Cassie-Baxter state. Considered f value for Cassie impregnating model according to (Eq. 1.3), the value is found as 16% (for θ_{CB}=140°). It means that greater than 84% of the water droplet is in contact with substrate while the other is on air [16].

2. Materials and Methods

The volcanic pumice samples were collected from the Geopark region, given in Figure 2a. There are two types of pumice as acidic and basic. The commonly used acidic pumice is light colored, whereas the basic one is dark colored [2]. It could be said that the pumice stone in Figure 2b is basic. All the chemicals in this study were analytical grade and used without further purification. Copper acetate and stearic acid were supplied by Sigma Aldrich and Chem Pure, respectively. Ethanol was from Merck. As shown in the literature, surfaces are given water repellency by means of various chemicals for low-surface energy modification, such as long alkyl chain thiols and fatty acids, aluminum and zirconium compounds, paraffin-based propellants, proteins, metal complexes, stearic acid compounds, fluorocarbons, silicone-based propellants, etc. [14]. Copper stearate (CSA) dispersion was used to give the property of hydrophobicity to the surface of the pumice in this study. For this aim, 0.75 grams of copper acetate was dissolved in 100 ml of ethyl alcohol. Considering the stoichiometric ratio between copper acetate and stearic acid, 2.37 grams of stearic acid (SA) was dissolved in 100 ml of ethyl alcohol. The SA solution was then added slowly to the copper acetate solution at 60ºC as stated in the previous study [18]. The surfaces of the volcanic pumice samples cut via scroll saw were covered using a spray bottle containing the resulting dispersion and allowed to dry in

the oven. The pumice sample covered with CSA is abbreviated as the CSA-pumice. In order to examine whether there is any effect of spray times (STs) on the contact angles of the CSA-pumice samples, the surfaces of the pumice samples were covered with spraying the CSA dispersion 2, 5, 10 and 20 times.

Figure 2. Photographs of the region (a) where the samples were taken in the Geopark region and a representative sample of the pumice stone (b).

2.1 Characterization

X-ray Fluorescence (XRF) spectroscopy analysis was made by Rigaku ZSX Primus II. Scanning Electron Microscopy (SEM) observations were carried out with QUANTA 400F Field Emission SEM after the samples were coated with Pd-Au on carbon film. Attension Theta Lite was used for contact angle measurements by creating a sessile drop from a liquid droplet at room temperature. The drop volume was approximately 10 μL. To determine whether contact angles are affected or not from the porous structure/STs of the CSA-pumice samples, five measurements were made at the regions of different porous structures on the samples. Fourier Transform Infrared Spectroscopy (FTIR) analyses of the CSA-pumice sample and the CSA dispersion were carried out using Perkin Elmer Spectrum Two in the range of 400–4000 cm^{-1} with ATR technique.

3. Results and discussion

3.1 Characterization of the volcanic pumice samples

Figure 3 shows XRF pattern of the pumice sample. Table 1 illustrates that SiO_2 is the major component (~43.0%) with about 18.80% Al_2O_3, determined depending on the pattern. In addition, various metal oxides (>1%) have been found in the structure of the pumice such as iron, calcium, sodium, potassium, magnesium and titanium oxides. This composition shows that the pumice has a polar character and tends to interact well with water via mainly dipole-dipole and ion-dipole interactions.

The strong peak around 1000 cm^{-1} in the FTIR spectrum (Figure 4) of the CSA-pumice in powder form corresponds to Si–O stretching vibrations. A twin peak between 2950 and 3600 cm^{-1} may show the existence of Cu co-planarity during Cu salt formation [19].

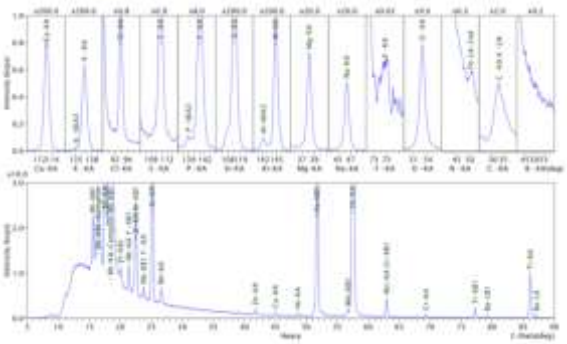

Figure 3. XRF pattern of the volcanic pumice sample.

Table 1. Chemical composition of the volcanic pumice determined by XRF.

No	Comp.	Result (% wt)	Det. limit	Intensity	w/o normal
1	SiO_2	43.0	0.0181	331.707	36.049
2	Al_2O_3	18.8	0.0113	194.629	15.742
3	Fe_2O_3	8.53	0.0053	269.248	7.149
4	CaO	7.77	0.0045	162.443	6.511
5	Na_2O	5.59	0.0155	9.766	4.685
6	CO_2	5.41	0.2154	0.756	4.532
7	K_2O	4.35	0.0033	124.059	3.649
8	MgO	3.11	0.0103	13.892	2.605
9	TiO_2	1.82	0.0115	9.354	1.524
10	P_2O_5	0.860	0.0030	12.055	0.721
11	MnO	0.185	0.0336	0.816	0.155
12	Cl	0.161	0.0033	1.127	0.135
13	SrO	0.139	0.0012	40.433	0.116
14	SO_3	0.130	0.0025	1.424	0.109
15	BaO	0.0874	0.0263	0.203	0.073
16	ZrO_2	0.0293	0.0069	2.251	0.024
17	Cr_2O_3	0.0187	0.0055	0.262	0.016
18	Nb_2O_5	0.0150	0.0016	5.253	0.013
19	Rb_2O	0.0106	0.0012	2.989	0.009
20	ZnO	0.0105	0.0018	0.896	0.009
21	NiO	0.0104	0.0023	0.518	0.009

The -CH stretchings of stearic acid in the spectrum of the CSA-pumice are seen in the range of 2800-2950 cm^{-1}. The peaks at 1589 and 1467 cm^{-1} were assigned to asymmetric and symmetric vibrations of the carboxylate group [20] due to the formation of copper stearate (Cu^{2+}+ $2CH_3(CH_2)_{16}COOH \rightarrow Cu[CH_3(CH_2)_{16}COO]_2 + 2H^+$) in the other study. These peaks are also seen at 1586 and 1515 cm^{-1} in the spectrum of the CSA-pumice. In addition, the observation of the small peak at 1691 cm^{-1} and of the shoulder at 1634 cm^{-1} for C=O vibrations could show the residue of stearic acid molecules/stearate ions interacting differently with Cu^{+2}/Si-O groups on the surface of the CSA-pumice.

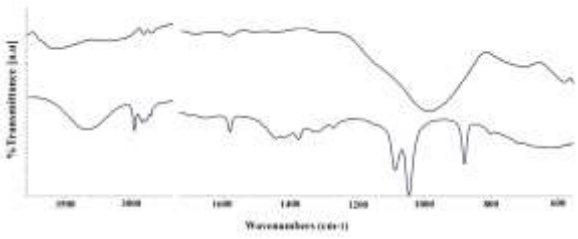

Figure 4. FTIR spectra of the CSA-pumice and the CSA dispersion in ethanol from top to down.

The FTIR spectrum of CSA dispersion involves some peaks [-OH (3335 cm^{-1}), C=O (1658, 1586 cm^{-1}), C-O (1047, 1088 cm^{-1}), C-H (2840-2980 cm^{-1}) etc.] belonging to the interactions between ethanol and stearic acid molecules. The FTIR measurements confirm covering of the pumice sample surface with mainly the CSA.

The SEM images of the pumice sample at different magnifications were given in Figures 5a-d. The images provide a better view of the pores/cavities that cannot be/can be seen with the naked eye and the rough structure throughout the surface as well as rod-like structures.

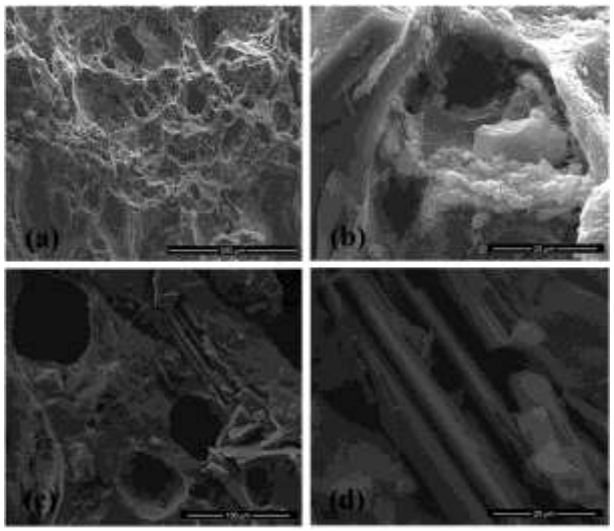

Figure 5. SEM images of the pristine pumice sample at different magnifications

Figure 6 shows SEM images of the CSA-pumice sample totally covered by the CSA dispersion. This coating has bur thorny flower-like morphology. In this morphology, thorny parts could involve mainly stearate groups when Cu^{+2} ions have been in the center of the flower. The size of a flower is about 15-20 µm. Different morphologies for SA coating have been observed in the literature depending on the treatment method, the treatment duration and the properties of pristine surface.

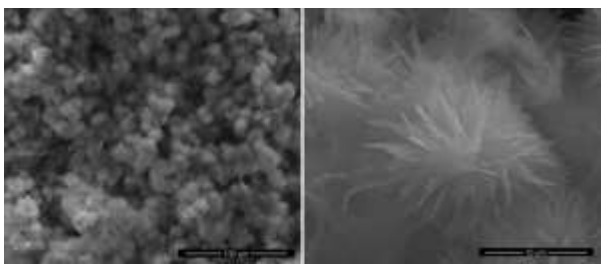

Figure 6. SEM images of the CSA-pumice sample at different magnifications

The formations of micro flowers of a diameter less than 5 µm (1 min) and of a rose-petal-like micro structured morphology (10 min) were observed from 1 min to 60 min in electrochemical modification of aluminum alloy in Cu/SA solutions [20]. The distribution of micro-nano flowers at anodic surface of the copper electrode after 1.5 h was seen in other study [21]. SEM image of super hydrophobic and super oleophilic poly(urethane) (PU) sponge prepared by facile dip coating in SA solution and subsequent heat treatment involved the micro/nanoscale SA protrusion with folding edges [22].

3.2 Wettability

Contact angle measurement is the main method in order to characterize the wettability of surfaces. When a water droplet forms a spherical shape, and the real contact between the adhered droplet and at surface is very small, a high contact angle (CA) occurs on the surface. In order for a surface to be super hydrophobic it must have a CA higher than 150°. In hydrophobic surface, the water drop will bead up with a CA greater than 90°. The wettable surfaces on which a water droplet tends to spread have a low CA value. Truly super hydrophilic surfaces possess roughness factors greater than one, and water spreads completely over them, which will have CA less than 5°. The drop will have a CA of less than 90° on hydrophilic surface [23-25].

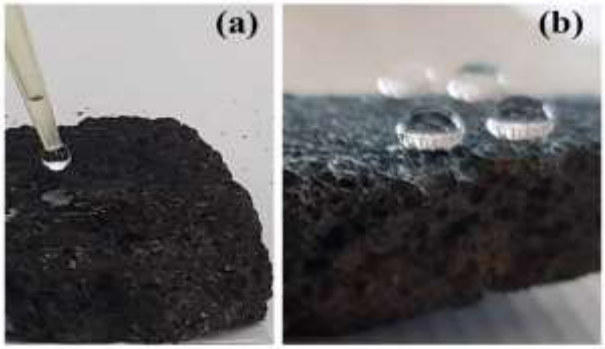

Figure 7. Wettability of the pristine pumice (a) and the CSA-pumice (b)

Figure 7 shows wettability of the pristine and the CSA-pumice samples. When water is dropped on the pristine pumice (Figure 7a), which has a rough structure and contains a large amount of metal oxide in its structure, water spreads completely and spreads over the entire surface by filling the pores/cavities of the rough surface. This shows that the pristine pumice has super hydrophilic nature, which suggests being in the Wenzel state. In the case of the CSA-pumice, it is observed in Figure 7b that the water drop remains on the sample, presenting non-sticking behavior. The pores in Figure 5 and Figure 7a may be getting smaller and more hydrophobic after being covered with CSA, nearly filled with the flowers (Figure 6).
More air could be trapped between the flowers in the pores on the CSA-pumice surface. The trapped air and

the CSA coating repel water drops and prevent them from spreading over the surface.

Figure 8. Sample images of water droplet CA measurements for the CSA-pumice sample (2 STs) from 141° to 117°.

Table 2. Summary of measured CA values for the CSA-pumice samples with different STs.

STs	CA values (°)
2	141, 131, 128, 121, 117
5	128, 121, 114, 111, 109
10	126, 116, 109, 108, 105
20	126, 121, 117, 112, 108

Sample images of the CA measurements are shown in Figure 8. The biggest CA value has been determined as 141° during the measurements taken from the regions of different porosity of the CSA-pumice sample covered with 2STs. The images imply that the CSA treatment imparted hydrophobic surfaces to the pumice samples. Yu et al. stated that the droplet is in the Cassie-Baxter state for hydrophobic textured surfaces generally only partially wetted [26]. The CA values in Table 2 show that the samples with different STs have different CAs in the same sample depending on the size of porosity. Chau et al. also stated that to obtain meaning and reproducible contact angle values of real samples is difficult, due to the surface property changing with many factors such as surface roughness, heterogeneity, particle size, and particle shape [27]. For these reasons it may not be possible to explain the effect of STs on the CA due to quite different CA values observed for each sample depending on heterogeneous porous structure of the pumice samples even if the highest CA value belongs to the sample with 2 STs. In another study, a decrease in CA was observed with an increase in concentration of stearic acid (SA) after 4 wt% in the case of SA-coated PU. This was attributed to the exposure of hydrophilic parts of SA molecules due to the hydrophobic association of long alkyl chain between the SA coating fixed to the PU sponge surface and the SA molecules, which were excessively absorbed at high SA concentration [22]. The CA value of the monolayer of SA obtained on mica by vapor exposure was 20°. Hydrophobicity was reached only when a thicker multilayer SA film (85° CA) was obtained in the study which involved the preparation of thin films of SA on mica by sublimation in air [28]. It is known that the CA values of flat surfaces even if coated with any material decreasing surface energy cannot exceed 120°.

Xu et al. [29] fabricated non-flaking 3D porous super hydrophobic frame with a pore size of less than 400 μm on copper foam substrates. Hierarchical micro-/nano-structures on the surfaces were obtained by immersing of the foams in ethanolic stearic acid solution at room temperature for about 4 days. The resulting material with the self-assembly CSA formation on Cu foam presented super hydrophobicity CA of 156°. In other studies that electrochemical modification was used for CSA/SA coating of any metal surface with/without etching, 162° [25] and ≈150° [15, 21] CA values were observed. The CA values increased from ∼125 to 151° depending on SA concentration from about 0.2 wt% to 4 wt%, and then decreased to about ∼147° in a study involving the PU sponge coated with SA [22]. The SA modification of the copper meshes/sheets caused 110° CA, after being abraded mechanically via SiC sandpaper various grits [30]. As seen in the literature, the differences between these CAs could also arise from the differences in surface chemical composition, porosity of the substrate, treatment methods and durations.

The techniques used in order to fabricate super hydrophobic surface usually involves two steps: roughening of the surface via etching chemically or mechanically to obtain micro-nano roughness and then modification of the surface to lower the surface energy [21]. The first step is not necessary when the volcanic pumice is used due to its rough morphology. Thus, using the volcanic sample as a starting material could be time-saving and inexpensive. However, the wide range of porous structures on the CSA-pumice surface may cause hydrophobicity instead of super hydrophobicity. The construction of the surface micro topography has great influence on the hydrophobic surfaces as Li et al. stated [30].

Wenzel's and Cassie-Baxter's equations help us to understand wettability properties of solid surfaces by accounting for their roughness and chemical structures. However, Erbil stated that much of the data in the literature are inconsistent with these theories and “modified forms” of Cassie's equations could be more convenient than others [31]. In our case, Cassie impregnating model may be used for the CSA-pumice sample involving the microstructures (the flowers) of about 15 μm on heterogeneous pores/cavities at its surface, possible macro/micro gaps between this microstructures depending on the size of pores/cavities and micro/nano gaps between the thorns of the flower. A water droplet may penetrates partially into the macro/micro gaps while not penetrate to the nano gaps. However, Chau et al. suggested to examine the detailed nature of the surfaces and characterize the surfaces to the smallest possible scale instead of trying to fit experimental data to idealized models in order to understand wetting phenomena of real surfaces. Thus, it may be possible to scale upwards to extract macroscopically verifiable data [27].

4. Conclusion

This study involves firstly the characterization of volcanic pumice samples from the Kula region. As can be seen from XRF and SEM analyses, the pumice samples consist of various oxides and have porous morphology. Having about 0º CA and facilitating water penetration into their pores quickly, the pristine pumice sample exhibits super hydrophilicity. Also as part of the study, the sample was treated with the CSA dispersion to see the effect of the treatment on wettability. In order to examine the effects of the treatment on the surface of the pristine one, the CSA-pumice sample has been examined via FTIR, SEM and CA measurements. The transformations in surface property and morphology of the pristine pumice with the CSA treatment have been shown via FTIR and SEM analyzes, respectively. The CA measurements have confirmed the change in the surface property of the pumice with the treatment from super hydrophilic to hydrophobic. The CSA-pumice samples have yielded CA values from 105 to about 141º due to their hydrophobic surfaces, the varying sizes of pores on their surface and various STs.

The wettability properties of the pristine and the treated pumice samples were tried to be explained in this study, depending upon their surface properties and the wettability models. The pristine pumice and the CSA-pumice samples may conform to Wenzel and Cassie impregnating models, respectively. Our next goal is to clarify how the spray coating with CSA influences on its surface porosity and roughness by examining the pore size distributions of the same pumice sample before and after coating with the CSA dispersion. It can be also examined whether reducing the SA concentration and covering the pristine pumice samples with various silanes will alter the results of this study.

Author's Contributions

Ruhan Benlikaya: Drafted and wrote the manuscript, assisted in analytical analysis on the structure, supervised the experiment's progress, and result analysis.
Mehmet Kahrıman: Performed the experiment, helped in result analysis.

Ethics

There are no ethical issues after the publication of this manuscript.

References

[1]. Dünyada ve Türkiye'de Pomza, Maden ve Teknik Arama Müdürlüğü. https://www.mta.gov.tr/v3.0/sayfalar/bilgi-merkezi/maden-serisi/pomza.pdf (accessed at 10.02.2021)

[2]. Çimen, Ö, Dereli, B, Keleş, E. 2020. Comparison of the effect of pumice of three different regions to high plasticity clay. *BEU Journal of Science*; 9(1): 427-433.

[3]. Grützner, T, Prelević, D, Akal, C. 2013. Geochemistry and origin of ultramafic enclaves and their basanitic host rock from Kula Volcano, Turkey. *Lithos*; 180-181: 58-73.

[4]. Isik-Gürsoy, D, Uğurlu, E, Oldeland, J. 2018. Plant communities, diversity and endemism of the Kula Volcano, Manisa, Turkey. *Plant Biosystems*; 150(5): 1046-1055.

[5]. Demir, T, Aytaç, A. 2019. Recommendation of three new geosites that are internationally significant in terms of geo-heritage within the territory of the Kula UNESCO Global Geopark. *Mediterranean Journal of Humanities*; 9: 125-140.

[6]. Hossain, KMA. 2004a. Properties of volcanic pumice based cement and lightweight concrete. *Cement and Concrete Research*; 34: 283-291.

[7]. Hossain, KMA. 2004b. Potential use of volcanic pumice as a construction material. *Journal of Materials in Civil Engineering*; 16 (6): 573-577.

[8]. Maleki, A, Gharibi, S, Valadi, K, Taheri-Ledari, R. 2020. Pumice-modified cellulose fiber: An environmentally benign solid state hybrid catalytic system for the synthesis of 2,4,5-triarylimidazole derivatives. *Journal of Physics and Chemistry of Solids*; 142: 109443.

[9]. Alemayehu, E, Lennartz, B. 2009. Virgin volcanic rocks: Kinetics and equilibrium studies for the adsorption of cadmium from water. *Journal of Hazardous Materials*; 169: 395-401.

[10]. Kitis, M, Kaplan, S, Karakaya, E, Yiğit, N, Civelekoglu, G. 2007. Adsorption of natural organic matter from waters by iron coated pumice. *Chemosphere*; 66: 130-138.

[11]. Yigit, NO, Tözüm Akgül S. 2012. Removal of selenium species from waters using various surface-modified natural particles and waste materials. *Clean (Weinh)*; 40 (7): 735-745.

[12]. Kaplan Bekaroğlu, S, Yigit, N, Karanfil, T, Kitis, M. 2010. The adsorptive removal of disinfection by-product precursors in a high-suva water using iron oxide-coated pumice and volcanic slag particles. *Journal of Hazardous Materials*; 183: 389-94.

[13]. Yayayürük, O, Erdem Yayayürük, A, Koçak, Ç, Koçak S. 2017. Lead and copper removal using Kula volcanics from environmental waters. *Separation Science and Technology*; 52(17): 2777-2787.

[14]. Erayman, Y, Korkmaz, Y. 2017. Süperhidrofob Tekstil Yüzeylerin Florsuz Bileşikler Kullanılarak Sol-Jel Yöntemi ile Modifikasyonu. *Tekstil ve Mühendis*; 24: 105: 41-52.

[15]. Bahrami, H, Ahmadi, B, Saffari, H. 2017. Preparing superhydrophobic copper surfaces with rose petal or lotus leaf property using a simple etching approach. *Material Research Express*; 4: 055014.

[16]. Jiaqiang, D, Jin, Y, Deng, Y, Zuo, W, Zhao, X, Han, D, Peng, Q, Zhang, Z. 2018. Wetting models and working mechanisms of typical surfaces existing in nature and their application on superhydrophobic surfaces: A review. *Advanced Materials Interfaces*; 5: 1701052–1701091.

[17]. Ebert, D, Bhushan, B. (2012) Wear-resistant rose petal-effect surfaces with superhydrophobicity and high droplet adhesion using hydrophobic and hydrophilic nanoparticles. *Journal of Colloid and Interface Science*; 384: 182-188.

[18]. Keyf, S. 2019. Responce surface with Box-Benhken design for hydrophobic copper stearate synthesis. *European Journal of Science and Technology*; (16): 834-840.

[19]. Anbarasan, R, Palanikumar, S, Devi, AA, Chen, P-H, Tung, KL. 2019. Characterization and application of Cu based superhydrophobic catalyst. *Progress in Natural Science*; 29 (4): 371-378.

[20]. Xu, N, Sarkar, D, Chen, X, Zhang, H, Tong W. 2016. Superhydrophobic copper stearate/copper oxide thin films by a simple one-step electrochemical process and their corrosion resistance properties. *RSC Advances*; 6: 35466-35478.

[21]. Huang, Y, Sarkar, D, Chen, XG. 2010. A one-step process to engineer superhydrophobic copper surfaces. *Materials Letters;* 64: 2722-2724.

[22]. Wang, J, Zheng, Y. 2017. Oil/water mixtures and emulsions separation of stearic acid-functionalized sponge fabricated via a facile one-step coating method. *Separation and Purification Technology*; 181: 183-191.

[23]. Koch, K, Barthlott, W. 2009. Superhydrophobic and superhydrophilic plant surfaces: An inspiration for biomimitric materials. *Philosophical Transactions of the Royal Society A: Mathematical*, *Physical and Engineering Science*; 367: 1487-1509.

[24]. Drelich, J, Chibowski, E, Meng, DD, Terpilowski, K. 2011. Hydrophilic and superhydrophilic surfaces and materials. *Soft Matter*; 7: 9804–9828.

[25]. Simpson JT, Hunter, SR, Aytug, T. 2015. Superhydrophobic materials and coatings: A review. *Reports on Progress in Physics*; 78: 086501.

[26]. Yu, D, Doh, S, Kwak, H, Kang, H-C, Ahn, HS, Park, HS, Moriyama, K, Kim, MH. 2015. Wetting state on hydrophilic and hydrophobic micro-textured surfaces: Thermodynamic analysis and X-ray visualization. *Applied Physics Letters*; 106: 171602.

[27]. Chau, TT, Bruckard, W, Koh, PTL, Nguyen, A, 2009. A review of factors that affect contact angle and implications for flotation practice. *Advances in colloid and interface science*; 150: 106-15.

[28]. Sauthier, G, Segura, J, Fraxedas, J, Verdaguer, A. 2014. Hydrophobic coating of mica by stearic acid vapor deposition. *Colloids and Surfaces A*: *Physicochemical* and *Engineering Aspects*; 443: 331–337.

[29]. Xu, J, Cao, Y, Ji, X, Yan, Y. 2013. Fabrication of non-flaking, superhydrophobic surfaces using a one-step solution-immersion process on copper foams. *Applied Surface Science*; 286: 220-227.

[30]. Li, Y, Yang, S, Chen, Y, Zhang D. 2020. Hydrophobic and anti-fouling performance of surface on parabolic morphology, *International Journal of Environmental Research and Public Health*; 17 (2) 644: 1-11.

[31]. Erbil, HY. 2014. The debate on the dependence of apparent contact angles on drop contact area or three-phase contact line: A review. *Surface Science Reports*; 69: 325-365.